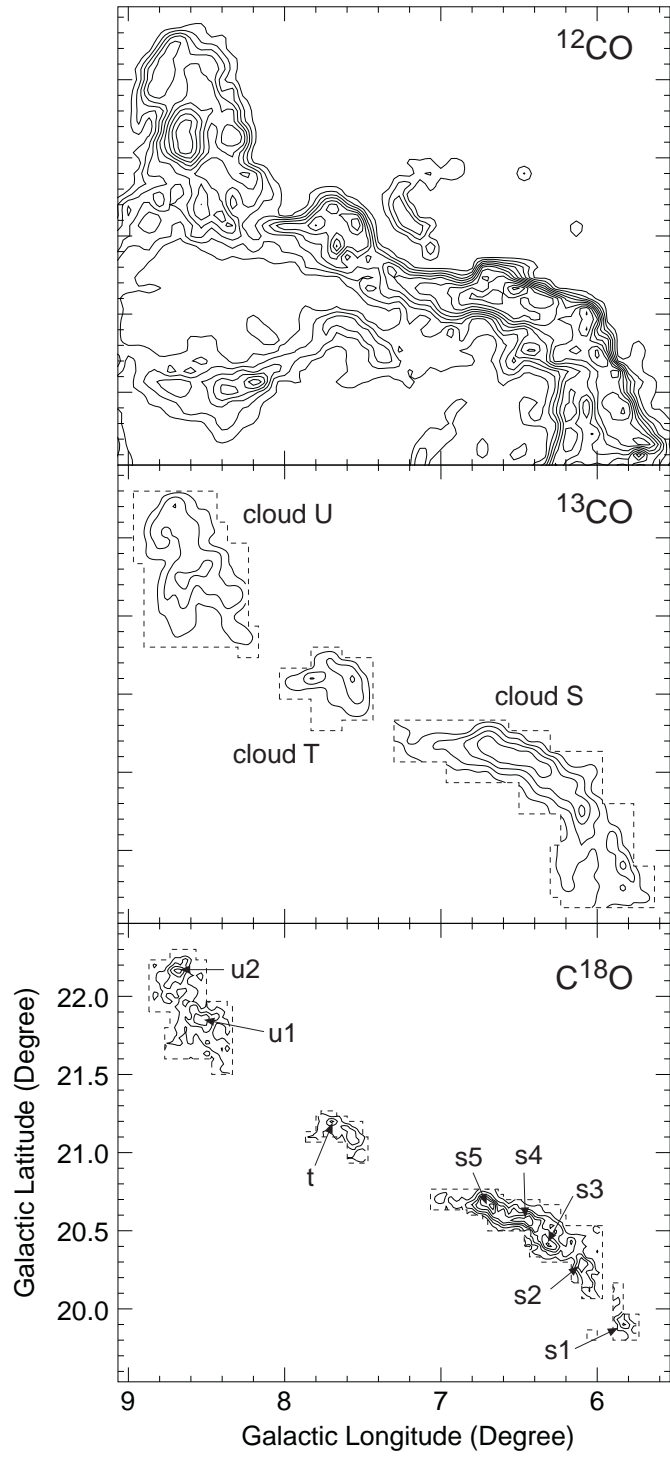


This figure "Fig1.gif" is available in "gif" format from:

<http://arxiv.org/ps/astro-ph/0007145v1>

This figure "Fig2.gif" is available in "gif" format from:

<http://arxiv.org/ps/astro-ph/0007145v1>



This figure "Fig4a.gif" is available in "gif" format from:

<http://arxiv.org/ps/astro-ph/0007145v1>

This figure "Fig4b.gif" is available in "gif" format from:

<http://arxiv.org/ps/astro-ph/0007145v1>

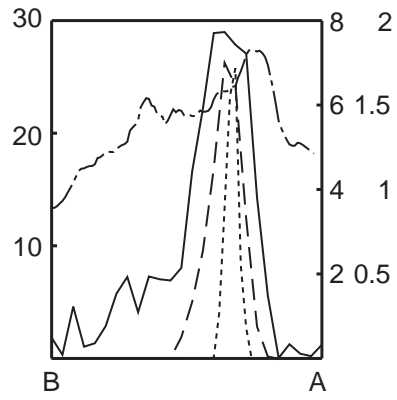
This figure "Fig5.gif" is available in "gif" format from:

<http://arxiv.org/ps/astro-ph/0007145v1>

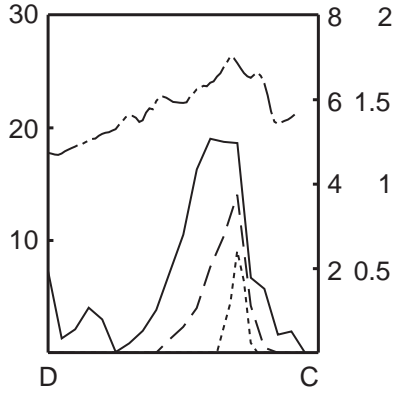
This figure "Fig6.png" is available in "png" format from:

<http://arxiv.org/ps/astro-ph/0007145v1>

(K Km s<sup>-1</sup>)



(K Km s<sup>-1</sup>)



(K Km s<sup>-1</sup>)

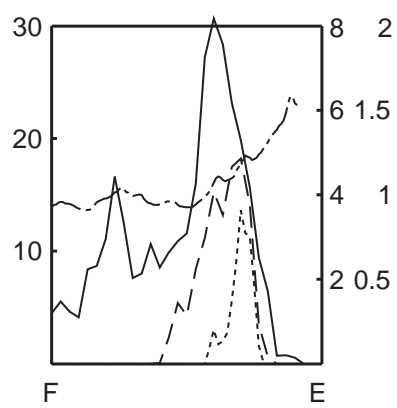


Table 1. Observed Properties.

cloud number	$l$ (deg)	$b$ (deg)	$\alpha$ (1950)			$\delta$ (1950)			Mass ( $M_{\odot}$ )	$a$ (pc)	$b$ (pc)	mean $N(\text{H}_2)$ ( $\times 10^{21} \text{ cm}^{-2}$ )	peak $N$ ( $\times 10^{21} \text{ cm}^{-2}$ )
			(hh)	mm	ss.s)	( $^{\circ}$	'	"					
1	5.000	23.467	16	31	56.9	-11	28	57.8	520	10.2	2.8	1.6	3.1
2	4.933	19.267	16	45	38.4	-14	1	56.7	200	4.2	1.4	2.3	3.5
3	6.533	20.667	16	44	36.3	-11	59	36.1	430	6.5	1.5	2.6	4.4
4	7.667	20.867	16	46	26.8	-11	0	49.7	70	2.0	1.7	2.5	3.3
5	8.600	21.600	16	46	2.0	-9	52	49.9	230	3.7	1.9	2.5	3.7
6	9.667	21.333	16	49	12.5	-9	12	52.7	100	3.1	1.4	2.1	2.6
7	8.200	20.067	16	50	17.1	-11	3	46.9	70	2.3	1.5	1.7	2.7

Table 2. Kinematics of the Clouds.

cloud number	$V_1$ ( $\text{km s}^{-1}$ )	$V_2$ ( $\text{km s}^{-1}$ )	$P$ ( $M_\odot \text{ km s}^{-1}$ )	$E$ ( $\times 10^{45}$ erg)	$\tau_{\text{E-SW}}$ ( $\times 10^5$ yr)	$\tau_{\text{P-SW}}$ ( $\times 10^8$ yr)	$dM/dt$ ( $\times 10^{-4} M_\odot \text{ yr}^{-1}$ )
1	-2.6	1.6	690	16.6	1.9	1.0	2.3
2	5.2	1.6	240	4.7	2.6	1.7	2.2
3	6.0	1.6	800	20.8	6.8	3.3	3.3
4	4.4	1.6	60	0.9	0.9	0.8	1.5
5	5.4	1.6	360	7.9	3.7	2.1	2.5
6	3.8	0.8	100	1.6	1.2	0.9	1.8
7	5.4	2.0	70	1.3	1.2	0.8	1.5

# Molecular Clouds Around a Run-away O Star, $\zeta$ Oph

Kengo TACHIYARA,<sup>1,2</sup> Rihei ABE,<sup>2</sup> Toshikazu ONISHI,<sup>2</sup> Akira MIZUNO,<sup>2</sup> and Yasuo FUKUI<sup>2</sup>

<sup>1</sup>*Max-Planck-Institut für extraterrestrische Physik, Giessenbachstraße, D-85748 Garching, Germany*  
*E-mail(KT): tatihara@mpe.mpg.de*

<sup>2</sup>*Department of Astrophysics, Nagoya University, Chikusa-ku, Nagoya 464-8602, Japan*

(Received January 24 2000; accepted June 21 2000)

## Abstract

Molecular clouds around a run-away O star  $\zeta$  Oph have been surveyed with NANTEN telescope and their streaming motion caused by  $\zeta$  Oph has been detected.  $\zeta$  Oph is the earliest (O9.5V) member of the Sco OB2 association and is a runaway star rapidly moving accompanied by an H II region S27. We detected 2 major filamentary cloud complexes; one complex including L156 (L156 complex) is lying across nearly the center of S27 and the other one (L204 complex) is located near the eastern edge of S27. Total masses of them traced by the  $^{12}\text{CO}$  emission in the two complexes are  $520 M_{\odot}$  and  $1110 M_{\odot}$ , respectively. Denser molecular cloud cores detected in  $\text{C}^{18}\text{O}$  are locally distributed on the near side of the L204 complex to  $\zeta$  Oph, and lower density gas traced by  $^{12}\text{CO}$  spreads toward the opposite side. Both complexes have radial velocity shifts that are correlated with the gas density. These spatial and velocity structures can be interpreted as follows; (1) the L156 complex is stuck on the expanding Strömgren sphere and has been accelerated, (2) the molecular gas in L204 complex was compressed and has also been accelerated outward from the H II region by  $\zeta$  Oph, resulting the radial velocity shifts of diffuse low-density gas relative to the dense cores embedded in the cloud.

These density and velocity structures indicate dynamical interaction between the H II region and the molecular clouds. The cloud complexes are divided into seven clouds by intensity distributions. In order to investigate the acceleration mechanism, we calculated momentum and kinetic energy for each cloud. They range from 60 to  $800 M_{\odot} \text{ km s}^{-1}$  and from  $0.9$  to  $21 \times 10^{45}$  erg, respectively. We examined the effects of the stellar wind and photo evaporation by UV field of  $\zeta$  Oph and found that the stellar wind can hardly input the momentum during the crossing time of the rapid movement of  $\zeta$  Oph. UV radiation seems to be a more likely origin of the streaming gas motion.

**Key words:** Interstellar: clouds — Interstellar: individual (Ophiuchus region, zeta Oph, L156, L204) — Interstellar: kinematics and dynamics — Interstellar: molecule — radio lines: Interstellar — stars: formation

## 1. Introduction

$\zeta$  Oph (HD149757; O9.5V type,  $\alpha_{1950} = 16^{\text{h}}34^{\text{m}}24^{\text{s}}.1$ ,  $\delta_{1950} = -10^{\circ}28'03''$ ) is the earliest star among the members of Sco OB2 association (de Geus et al. 1989). The bright UV and optical light of the star provide good opportunities to study foreground diffuse interstellar medium in many emission and absorption lines of various molecules and atoms, and chemical composition has been derived (e.g., Morton 1975, Langer et al. 1987, Kopp et al. 1996, and Liszt 1997).  $\zeta$  Oph itself is ionizing a density-bound H II region, S27, which spreads in an elliptical shape of  $\sim 7^{\circ} \times 10^{\circ}$  in  $\alpha$  and  $\delta$  (Morgan et al. 1955), corresponding to  $\sim 18 \text{ pc} \times 26 \text{ pc}$  at a distance of 140 pc. Some of the extinction features shading the  $\text{H}\alpha$  emission are seen in a plate taken by Sivan (1974) which represents the existence of dark clouds in the foreground of

S27. These features coincide with the dark clouds L156, L204, L190, and so on (Lynds 1962), and clouds may be interacting with the H II region.

Physical interactions between early type stars and molecular clouds should be important processes related to formation, evolution, and dissociation of molecular clouds.  $\zeta$  Oph and its surroundings are one of the best sites to investigate these interactions because of its proximity to the sun. The distance to the star is estimated to be 200 pc (Lesh 1968), 170 pc (Bohlin 1975), and 140 pc (Draine 1986).  $\zeta$  Oph is also known as a rapidly moving run-away star, and the proper motion is measured as  $\mu_{\alpha*} = 0.013'' \text{ yr}^{-1}$ ,  $\mu_{\delta} = 0.025'' \text{ yr}^{-1}$  (Perryman et al. 1997). The helio-centric radial velocity of  $\zeta$  Oph is  $-10.7 \text{ km s}^{-1}$  (Lesh 1968) and a space velocity with respect to the local standard of rest (LSR) is  $3.3 \text{ km s}^{-1}$  in the radial direction,  $31.2 \text{ km s}^{-1}$  in the direction of in-

creasing  $l$ , and  $5.0 \text{ km s}^{-1}$  in the direction of increasing  $b$  (Draine 1986).  $\zeta$  Oph, therefore, has passed through the Ophiuchus region for a few millions years. This implies that the molecular clouds may have experienced being illuminated by strong UV light in a short time scale, and this gives us an ideal laboratory to study the physical interaction between molecular clouds and an early type star.

McCutcheon et al. (1986) made mm-wave observations in the  $J = 1-0$   $^{12}\text{CO}$  and  $^{13}\text{CO}$  emission toward L204, and found that the cloud has velocity structures which correlate with spatial distribution of the bent filament. They suggested that the filamentary cloud is influenced by external compression, possibly due to  $\zeta$  Oph, resulting in the velocity structure and the morphology of the cloud. The spatial and density coverage is, however, limited and more extensive observations with wide density regime are needed to reveal the dynamical interaction. They also showed that the optical polarization vectors are aligned perpendicular to the long axis of L204, which suggests the magnetic fields penetrating the filamentary cloud perpendicularly. Heiles (1988) estimated the magnetic field strength from the HI Zeeman splitting to be  $\sim 12 \mu\text{G}$ .

Nozawa et al. (1991) made extensive  $^{13}\text{CO}$  observations covering the entire Ophiuchus North region and revealed large scale cloud distribution. There are 3 molecular clouds identified in an area of  $\sim 10 \text{ deg}^2$  around  $\zeta$  Oph, while only one young stellar object is found to be physically associated there. They conclude that the Ophiuchus North region is inactive in star formation despite of the existence of massive molecular gas of  $\sim 4400 M_{\odot}$ . Subsequently, denser gas distributions were studied by Tachihara et al. (2000) with  $\text{C}^{18}\text{O}$  observations, that found the dense cloud cores whose average density is  $\sim 10^4 \text{ cm}^{-3}$  embedded in the molecular clouds.

In order to reveal the dynamical interaction in the region of  $\zeta$  Oph and to investigate how it affects the cloud structure and dynamics, we have made extensive  $^{12}\text{CO}$  molecular line observations toward the region. In section 2, we briefly summarize the observational properties and spatial and velocity distributions, and the physical parameters of the detected clouds are mentioned in section 3. Section 4 discusses the dynamical interaction between  $\zeta$  Oph and the molecular clouds by introducing the calculations of kinematic energy and momentum. Finally, the summary of this paper is given in section 5.

## 2. Observations

An area of  $\sim 47 \text{ deg}^2$  around  $\zeta$  Oph and S27 has been observed in  $^{12}\text{CO}$  ( $J = 1-0$ ) emission line (115.2 GHz) with the NANTEN millimeter wave telescope (HPBW =  $27'$ ) at Las Campanas observatory. In total, 10575  $^{12}\text{CO}$  spectra were obtained with  $4'$  grid spacing. Velocity resolution of each spectrum is  $\sim 0.1 \text{ km s}^{-1}$ , and velocity

coverage is  $100 \text{ km s}^{-1}$  centered at  $5 \text{ km s}^{-1}$ . Absolute antenna temperature was calibrated by adopting the peak  $T_{\text{r}}^*$  of  $\zeta$  Oph East, *IRAS* point source 16293–2422, as 15 K. The typical integration time for each observed point was  $\sim 5$  sec, and rms noise temperature after the calibration is  $\sim 0.56 \text{ K}$  for  $0.1 \text{ km s}^{-1}$  velocity resolution.

To investigate the denser region of the molecular cloud, L204 was observed also in  $^{13}\text{CO}$  ( $J = 1-0$ ) emission line (110.20137 GHz) with the 4m millimeter wave telescope installed in Nagoya University, and 491  $^{13}\text{CO}$  spectra were obtained with  $4'$  grid spacing. Velocity resolution is the same as above. The intensity scale of  $^{13}\text{CO}$  spectra were calibrated referring  $T_{\text{r}}^*$  of M17SW as 14.7 K (Nozawa et al. 1991). In order to compare dense cores embedded in the cloud,  $\text{C}^{18}\text{O}$  data were also obtained with the same telescope for the intense parts of the  $^{13}\text{CO}$  emission with  $2'$  grid spacing (Tachihara et al. 2000). The total number of  $\text{C}^{18}\text{O}$  spectra obtained in this region is  $\sim 940$ .

## 3. Results

### 3.1. Overview of the $^{12}\text{CO}$ distribution

The integrated intensity of the  $^{12}\text{CO}$  ( $J = 1-0$ ) emission is shown in Fig. 1. Two major filamentary complexes exist lying from the north to the south. The western one runs along  $\alpha = 16^{\text{h}}33^{\text{m}}$  crossing through the center of the HII region with  $\sim 10\text{-pc}$  length and  $\sim 3\text{-pc}$  width. Some dark clouds including L156, L145, and L121 were identified inside of this complex (hereafter L156 complex).  $\zeta$  Oph exists at  $\sim 1$  degree north of the center of L156 complex and the  $^{12}\text{CO}$  intensity toward the star is apparently weaker than the other parts. Another cloud complex (hereafter L204 complex) has a curved filamentary structure of  $\sim 20\text{-pc}$  length and  $\sim 2\text{-pc}$  width as a whole, being located near the eastern boundary of the HII region. Some  $^{12}\text{CO}$  peaks are also embedded in places, being connected by filamentary clouds. Diffuse components spread toward the east of the L204 complex. Little CO emission is, however, detected between the 2 complexes. At the western edge of the L204 complex, a large intensity gradient is shown by tight contour lines, suggesting a relatively large density gradient there. The  $^{12}\text{CO}$  integrated intensity is stronger in the L204 complex than in the L156 complex on the whole; the strong intensity at the clumpy regions in the L204 complex is especially prominent.

### 3.2. Physical parameters

L204 complex is divided into 6 clouds bordered by less intense bridges (see Fig. 2). Regarding L156 complex as one cloud, we estimate physical parameters for each cloud as show in Table 1. In general,  $^{12}\text{CO}$  ( $J = 1-0$ ) emission is optically thick. It becomes saturated when the  $\text{H}_2$  col-

umn density,  $N(\text{H}_2)$ , is larger than  $10^{21} \text{ cm}^{-2}$ , and may not reflect the actual  $N(\text{H}_2)$ . Nonetheless, we estimate physical parameters of  $N(\text{H}_2)$ , mass, and density using an empirical relation,  $N(\text{H}_2) = W(^{12}\text{CO}) \times 1.56 \times 10^{20} \text{ cm}^{-2}$  (Hunter et al. 1997) where  $W(^{12}\text{CO})$  is the integrated intensity of CO emission. Note that this conversion factor may change from region to region according to the circumstances. In the region with strong UV field, the value is expected to be larger because of higher degree of CO dissociation. It is, however, very difficult to estimate the factor for each cloud, so here we assume that it is uniform all through the region. In this sense,  $N(\text{H}_2)$  and mass give the lower-limit values. Cloud positions are defined as the peak intensity position in galactic and equatorial coordinates (B1950). The cloud mass is derived by summing up the  $N(\text{H}_2)$  of all the observed points where  $W(^{12}\text{CO})$  is greater than  $1.2 \text{ K km s}^{-1}$  ( $= 3 \sigma$ ). The total mass of the 7  $^{12}\text{CO}$  clouds is then calculated to be  $1630 M_\odot$ . The Average  $N(\text{H}_2)$  is also estimated within the area where  $W(^{12}\text{CO}) \geq 1.2 \text{ K km s}^{-1}$  for each cloud. Peak  $N(\text{H}_2)$ ,  $T_r^*$ ,  $\Delta V$ , and  $V_{\text{LSR}}$  are measured at the most intense position of each cloud and  $T_r^*$ ,  $\Delta V$ , and  $V_{\text{LSR}}$  are estimated by fitting the spectral date to a single gaussian profile. The total mass of the whole observed area, where  $W(^{12}\text{CO}) \geq 1.2 \text{ K km s}^{-1}$ , is  $2140 M_\odot$ .

### 3.3. Distribution of $^{13}\text{CO}$ clouds and $\text{C}^{18}\text{O}$ cores

Fig. 3 represents a comparison among the distributions of integrated intensity in  $^{12}\text{CO}$ ,  $^{13}\text{CO}$ , and  $\text{C}^{18}\text{O}$  in L204 complex. The  $J=1-0$   $^{13}\text{CO}$  and  $\text{C}^{18}\text{O}$  spectra generally trace relatively denser regions of  $\sim 10^3 \text{ cm}^{-3}$  and  $\sim 10^4 \text{ cm}^{-3}$ , respectively. The  $^{13}\text{CO}$  emission is distributed as 3 distinct clouds which coincide with the previously identified clouds, S, T, and U by Nozawa et al. (1991), respectively. They are localized in the filamentary ridge of  $^{12}\text{CO}$  where  $W(^{12}\text{CO}) \geq 8 \text{ K km s}^{-1}$ . The 3  $^{13}\text{CO}$  clouds have masses of 500, 75, and  $220 M_\odot$ , respectively. Tachihara et al. (2000) identified 8 cores in this region in  $\text{C}^{18}\text{O}$  (Fig. 3c). These  $\text{C}^{18}\text{O}$  cores have clumpy shapes in general. Cloud S has an arc-like structure and the  $\text{C}^{18}\text{O}$  cores are aligned on the outer edge of the arc. Cloud U has a ‘‘bullet’’-like structure and the  $\text{C}^{18}\text{O}$  core is located at the ‘‘head’’. The  $\text{C}^{18}\text{O}$  cores tend to be distributed relatively closely to  $\zeta$  Oph in the  $^{12}\text{CO}$  and  $^{13}\text{CO}$  clouds. Only one protostellar-like *IRAS* point source, 16442–0930, exists in this region and it appears to be associated with the core u2. This suggests that star formation is taking place in the core. The densest regions in these clouds have  $N(\text{H}_2)$  of  $\sim 1.1 \times 10^{22} \text{ cm}^{-2}$  (peak position of core s5) as measured by  $\text{C}^{18}\text{O}$ .

### 3.4. Velocity fields of the clouds

The  $^{12}\text{CO}$  clouds show a velocity change from  $\sim -3.0 \text{ km s}^{-1}$  to  $\sim 7.8 \text{ km s}^{-1}$  and the velocity channel maps are shown in Figs. 4. Each map shows integrated intensity of  $^{12}\text{CO}$  with a velocity width of  $0.6 \text{ km s}^{-1}$ . Together with Fig. 5, it is seen that the 2 complexes have different velocity components. The L156 complex has a more negative velocity ranging from  $-3 \text{ km s}^{-1}$  to  $1.8 \text{ km s}^{-1}$ , while L204 complex a more positive one from  $1.2 \text{ km s}^{-1}$  to  $7.8 \text{ km s}^{-1}$ . On the other hand, each complex has its own internal velocity structures.

First, the L156 complex has the smallest velocity of  $-2.0 \text{ km s}^{-1}$  at the middle of the filament,  $l \simeq 4^\circ 5', b \simeq 22^\circ 5'$ , that is  $\sim 2^\circ$  south from  $\zeta$  Oph. The velocity has a gradual change to  $1 \text{ km s}^{-1}$  from this position of the apex in the velocity field to the both ends of the filament.

Second, the L204 complex has a complicated velocity structure whose peak velocity ranges from  $1.2 \text{ km s}^{-1}$  to  $7.8 \text{ km s}^{-1}$  as a whole and each cloud has its unique velocity structure. Cloud 2 has the largest velocity of  $\sim 5 \text{ km s}^{-1}$  at the most western position (upper right in the figures) and the peak position changes to the east with the velocity decreasing down to  $\sim 2.4 \text{ km s}^{-1}$ . Cloud 3 has the largest velocity of  $\sim 5.5 \text{ km s}^{-1}$  at the position where the  $\text{C}^{18}\text{O}$  cores s4 and s5 exist, and the intense regions change to  $\sim 1.5 \text{ km s}^{-1}$  toward both sides along the filament. Cloud 5 has a velocity structure similar to cloud 2 and has the largest velocity of  $\sim 5.4 \text{ km s}^{-1}$  at the position of the  $\text{C}^{18}\text{O}$  core, u1. A general trend can be seen in the L204 complex that the densest part of the cloud has the largest velocity in each cloud and the smaller velocity components spread toward the less denser regions away from  $\zeta$  Oph. These features show strong indication of the dynamical interaction between molecular clouds and  $\zeta$  Oph as discussed in section 4.

## 4. Discussion

### 4.1. Physical Interaction between the clouds and $\zeta$ Oph

As shown by the morphology and velocity structure of the molecular clouds, the clouds seem to be interacting with  $\zeta$  Oph and/or its surrounding H II region. The clouds, cloud cores, and star formation are expected to be affected by  $\zeta$  Oph. It is known by the previous studies that star formation is inactive around  $\zeta$  Oph, although sufficiently dense and massive clouds and cloud cores exist (Nozawa et al. 1991; Tachihara et al. 2000). Magnetic fields are suggested to play an important role for cloud dynamics (McCutcheon et al. 1986, Heiles 1988) and the turbulent energy input from  $\zeta$  Oph to the molecular clouds should be taken into account as well in considering star formation.

In order to investigate the density and temperature distributions of a cloud qualitatively, we shall compare

the distributions of  $^{12}\text{CO}$ ,  $^{13}\text{CO}$ ,  $\text{C}^{18}\text{O}$ , and  $100\ \mu\text{m}$  far-infrared emission. Fig. 6 shows the intensity distribution of *IRAS*  $100\ \mu\text{m}$  emission overlaid with the contour of  $^{12}\text{CO}$  clouds. We investigate the intensity distributions of the  $^{12}\text{CO}$ ,  $^{13}\text{CO}$ ,  $\text{C}^{18}\text{O}$ , and  $100\ \mu\text{m}$  along 3 strip lines of A-B, C-D, and E-F illustrated by the blue lines in Fig. 6, as show in Figs. 7a-c. The 3 kinds of CO distributions all show the steeper gradients toward  $\zeta$  Oph.  $^{13}\text{CO}$  and  $\text{C}^{18}\text{O}$  are distributed locally close to  $\zeta$  Oph and  $^{12}\text{CO}$  spreads to the opposite sides. On the other hand, the  $100\ \mu\text{m}$  peaks at the closer edge of the clouds to  $\zeta$  Oph. These features can be explained by the compression of the clouds by  $\zeta$  Oph or by the surrounding H II region, denser cores are formed on the front side, and lower density gas may be accelerated to the opposite side toward the east. The front sides of the clouds facing  $\zeta$  Oph are illuminated by the UV light from  $\zeta$  Oph, and the dust temperature may increase. Thus the  $100\ \mu\text{m}$  emission is significantly enhanced on the front sides, suggesting that the gas and dust in this region may be compressed, accelerated and heated by  $\zeta$  Oph.

The  $100\ \mu\text{m}$  emission is relatively weaker toward the L156 complex than toward the L204 complex as well as the CO intensity. The former lies on the H II region nearly across the center while the latter at the boundary. The shadowing of the  $\text{H}\alpha$  emission clearly shows that clouds are located in front of the H II region (Sivan 1974). Because the L204 complex has larger radial velocity and  $N(\text{H}_2)$  than L156 complex has, the following geometrical and kinematic structures are suggested; i.e., the 2 complexes are sheet-like molecular clouds sticking on the expanding H II region being pushed by  $\zeta$  Oph. The L156 and L204 complexes are face-on and almost edge-on to us, respectively, and the projection effect makes the radial velocity and  $N(\text{H}_2)$  larger for the L204 complex. If it is the case, the smallest velocity position on the L156 complex is the nearest to us. Though it is actually  $\sim 2^\circ$  south from the  $\zeta$  Oph as mentioned above, it is explained by the rapid proper motion of  $\zeta$  Oph. About  $2.5 \times 10^5$  yr ago,  $\zeta$  Oph existed by  $\sim 30'$  closer to the position of the smallest velocity in L156 complex ( $l \sim 4^\circ 5'$ ,  $b \sim 22^\circ 5'$ ). The existence of some T Tauri stars (Nozawa et al. 1991) shows that the molecular clouds are preexistent and have formed stars prior to the passage of  $\zeta$  Oph, and now we see the results of interaction between  $\zeta$  Oph and the pre-existent molecular clouds.

As mentioned in Sec. 3.4, in L204 complex the lower density gas has smaller radial velocity and spread over far from  $\zeta$  Oph. This can be interpreted as molecular gas being pushed by some effects due to  $\zeta$  Oph; gas at the near side of the cloud to  $\zeta$  Oph is compressed and denser cores have been formed. Some fraction of the gas has been tone off from the cloud. The denser and more massive cloud cores can hardly be moved while the low-density gas can easily be accelerated. It is likely that the L204 complex

had simpler velocity structures and that the gas and dust were not affected dynamically prior to the passage of  $\zeta$  Oph. Since  $\zeta$  Oph approached to the clouds, the complicated velocity fields may have resulted. Around the inter-cloud region between the 2 complexes, faint string-like features in  $100\ \mu\text{m}$  running nearly perpendicular to the filamentary complexes can be seen, although no CO emission is detected perhaps due to low column density there. These strings are also prominent in the east of the L204 complex as traced by the strip lines A-B, C-D, and E-F, and they are nearly parallel to the projected magnetic fields (McCutcheon et al. 1986). This suggests that some of the gas and dust are tone off from the clouds and flowing to the downstream along the magnetic fields.

We also note that the  $^{12}\text{CO}$  emission is significantly weak toward  $\zeta$  Oph. This may be because a large fraction of CO molecules are dissociated by UV light. In the inter-cloud regions and cloud boundaries facing  $\zeta$  Oph, there must be photo-dissociation regions (PDRs) and CO molecules cannot be detected from such regions. This dissociation can also make the steep intensity gradients by the UV light penetrating into the cloud from the outside.  $N(\text{H}_2)$  and the cloud mass traced by CO represent the quantities only for the dense part of the molecular cloud where UV flux is effectively shielded by interstellar dust. In this sense, the obtained values of  $N(\text{H}_2)$  and mass should be regarded as the lower bounds as mentioned in Sec. 3.2. Observations of other tracers like C I and C II emission with high spatial resolutions are required to estimate the gas density in PDR more accurately.

#### 4.2. Energetics of the cloud motion and the origin of the kinematic energy input

To understand the physical interaction between  $\zeta$  Oph and the molecular clouds quantitatively, kinetic energy and momentum of the clouds are investigated. First, we assume that the gas component with the smallest velocity of cloud 1 and those with the largest velocity of clouds 2-7 are at rest and the gas with the other velocity component is flown away from the remaining gas due to the effects of  $\zeta$  Oph. The momentum,  $P$ , and the kinetic energy,  $E$ , are estimated for each cloud as follows;

$$P = \sum_{V=V_1}^{V_2} M_V |V - V_1|, \quad (1)$$

$$E = \frac{1}{2} \sum_{V=V_1}^{V_2} M_V (V - V_1)^2, \quad (2)$$

where  $V$  is the radial velocity, and  $M_V$  is the mass contained in the channel at  $V$ . Taking the  $V_1$  and  $V_2$  as the rest velocity and the velocity of the most highly accelerated component of each cloud, respectively,  $P$  and  $E$  are obtained as shown in Table 2. The total  $P$  and  $E$  of all the clouds amount to  $2330 M_\odot \text{ km s}^{-1}$  and  $5.4 \times 10^{46}$  erg,

respectively. As the dynamical effect for the compression and acceleration of the gas due to  $\zeta$  Oph, the stellar wind and UV radiation will be considered in the following.

First, the energy and the momentum input by the stellar wind (SW) will be discussed. If we accept the physical parameters of O9.5V type  $\zeta$  Oph that the SW has  $dm/dt \simeq 10^{-7} M_{\odot} \text{ yr}^{-1}$  and  $V_0 \simeq 1200 \text{ km s}^{-1}$  (Morton 1975), where  $dm/dt$  and  $V_0$  are the mass-loss ratio and the escape velocity, respectively, the total energy and momentum of the SW for a period of  $\tau$  yr are obtained as  $E_{\text{SW}} = \tau \times (1/2)(dm/dt)V_0^2 = \tau \times 1.5 \times 10^{42} \text{ [erg]}$  and  $P_{\text{SW}} = \tau \times (dm/dt)V_0 = \tau \times 1.2 \times 10^{-4} [M_{\odot} \text{ km s}^{-1}]$ , respectively. We assume here that clouds are of prolate shapes with the axial lengths listed in Table 1. The area exposed to the wind is then expressed as  $\pi ab$ , where  $a$  and  $b$  are major and minor axes of the cloud, respectively. The energy and momentum input to the cloud is expressed as  $E_{\text{SW}} \times (\pi ab)/(4\pi d^2)$  and  $P_{\text{SW}} \times (\pi ab)/(4\pi d^2)$ , respectively where  $d$  is the distance between  $\zeta$  Oph and the cloud. Thus, the expected time scales for energy and momentum input ( $\tau_{\text{E-SW}}$  and  $\tau_{\text{P-SW}}$ , respectively) are calculated independently for each cloud as listed in Table 2.

Next, we investigate the photo-dissociation effect by the UV flux of  $\zeta$  Oph. When a molecular cloud is illuminated by UV light, molecular gas will be evaporated away from the cloud with supersonic velocity, injecting momentum into the cloud. The cloud is then pushed backward as so-called the ‘‘rocket effect’’ (e.g., Oort & Spitzer 1954). The kinetic energy input by the evaporated gas is roughly calculated as follows; the number of Lyman photons per each second radiated by  $\zeta$  Oph is given as  $1.2 \times 10^{48} \text{ s}^{-1}$  (Panagia 1973). When we assume that all the clouds are on the Strömngren sphere at  $\sim 11$  pc away from  $\zeta$  Oph, the Lyman photon flux on the cloud surface,  $J_{\text{L}}$ , is estimated to be  $8.3 \times 10^7 \text{ cm}^{-2} \text{ s}^{-1}$ . The particle density of ionized gas,  $n_i$ , and  $J_{\text{L}}$  have a relation of

$$J_{\text{L}} = 0.01\alpha n_i^2 r_i \frac{m_i^2 + 1}{m_i^2 - 1}, \quad (3)$$

where  $m_i$  is the Mach number of the streaming gas,  $r_i$  the spherical cloud radius, and  $\alpha$  the recombination coefficient (Kahn 1969). Here we take  $m_i = 2$ ,  $\alpha = 2 \times 10^{-13}$  (Reipurth 1983) and  $r_i^2 = ab$ ,  $n_i$  can be calculated for each cloud. The mass loss rate from a cloud hemisphere illuminated by UV is expressed as

$$\frac{dM}{dt} = \pi ab \mu_i n_i v, \quad (4)$$

where  $\mu_i$  and  $v$  are particle mass ( $1.4m_{\text{H}}$ ) and escape velocity, respectively. If we take  $v = 20 \text{ km s}^{-1}$  according to Oort & Spitzer (1954), the mass loss rates of the clouds are estimated as listed in Table 2. By using this, the energy input by photo dissociation can be

expressed as  $E_{\text{PD}} = 1/2(dM/dt)v^2\tau_{\text{E-PD}}$  where  $\tau_{\text{E-PD}}$  is the time scale of photo dissociation. Also for the momentum,  $P_{\text{PD}} = (dM/dt)v\tau_{\text{P-PD}}$ . Assuming the kinetic energy and momentum of the clouds are made only by this rocket effect, we estimate  $\tau_{\text{E-PD}}$  and  $\tau_{\text{P-PD}}$  as listed in Table 2.

The above two estimations are given as lower limits for the time scales because we assume that the momentum- and energy-transfer coefficients are 100%, the tangential velocity of the flowing gas is neglected, and the UV shielding effect by dust grains is also neglected. Nonetheless, these analyses tell us some information about the gas motion. For some of the clouds, the energy input by SW needs a time scale,  $\tau_{\text{E-SW}}$ , of only a few  $\times 10^5$  yr or less, that is comparable with the crossing time of  $\zeta$  Oph,  $\tau_*$ , through the clouds (see Fig. 5). However, the time scales required for the momentum input range around  $10^8$  yr and are significantly larger than  $\tau_*$ . Thus, we conclude that the stellar wind can hardly drive the high velocity gas in relatively short timescale of  $\tau_*$ . An  $U$ -shaped bow shock around  $\zeta$  Oph was found in [O III] (5010 Å) and 60  $\mu\text{m}$  bands (Gull & Sofia 1979; Van Buren & McCray 1988). This seems to be a partial shocked distorted bubble which is driven by SW. The size of the bubble is expected to be smaller than a few pc, which is significantly less than the distance to the clouds, since the expansion time scale is only a few  $\times 10^5$  yr (Weaver et al. 1977). This also supports the result, because SW cannot affect the clouds penetrating through the bow shocks. On the other hand, the rocket effect by UV photo dissociation is more likely the cause of the peculiar velocity structures in the cloud. The required time scales for both the kinetic energies and momenta are less than  $\tau_*$  and seem to be reasonable. Here we conclude that the rocket effect may be one of the possible mechanism of the gas acceleration.

#### 4.3. Possible origin of the turbulence in molecular cloud

Generally speaking, interstellar molecular gas is highly turbulent as inferred from the significantly larger molecular linewidth than the thermal one. It is also a general trend that denser gas has a smaller linewidth, roughly speaking,  $\sim 10 \text{ km s}^{-1}$  for H I gas,  $\sim 2 \text{ km s}^{-1}$  for  $^{12}\text{CO}$ ,  $\sim 1 \text{ km s}^{-1}$  for  $^{13}\text{CO}$ , and  $\sim 0.5 \text{ km s}^{-1}$  for  $\text{C}^{18}\text{O}$ . Recent studies revealed that the turbulent motion of gas may play an important role in cloud dynamics and star formation (Dobashi et al. 1996; Yonekura et al. 1997; Kawamura et al. 1998; Tachihara et al. 2000). Among all, Tachihara et al. (2000) suggest that the turbulence decay may lead to further contraction of cloud cores. Since most of the cores in Ophiuchus North region are starless, there must be no disturbance from YSO formed in the cores. As shown in detail by Nakano (1998), it is difficult to excite the turbulence in the cores from outside by magnetic field lines. Thus, the turbulence may be monotoni-

cally dissipated in time through the dynamical evolution of a core. If this is the case, the amount of turbulent energy of the original diffuse gas cloud and the dissipation rate of the turbulence are essential factors in the core evolution. As shown in the previous section, the photo dissociation by UV light is one of the probable causes of the turbulence. Since  $\zeta$  Oph is a run-away star crossing Ophiuchus region for about a few millions years, it may have disturbed the interstellar gas and put a significant amount of turbulent energy into all the clouds preexisting in the region during its travel. There are a few tens of OB stars in the Sco OB2 association and the contribution of the rest of these OB stars should not be neglected. The field strength of the total UV radiation is estimated to be an order of magnitude larger than the typical value for the Galactic plane (Nozawa et al. 1991). This may explain why the star formation in the Ophiuchus North region is very inactive. De Geus (1992) and Preibish & Zinnecker (1999) present a scenario that a massive star in Upper Sco exploded as a supernova about 1.5 Myr ago. A shock wave dispersed the clouds in the vicinity of the explosion and has compressed the  $\rho$  Oph cloud core, inducing the extremely active star formation in the  $\rho$  Oph cloud core. We can see an expanding HI shell centered at  $l \sim 345^\circ$  and  $b \sim 25^\circ$ , at whose boundary the  $\rho$  Oph cloud exists (de Geus 1992). The shock wave has not, however, reached the Ophiuchus North region (Tachihara et al. 1996). When we trace the position of  $\zeta$  Oph back to 1.5 Myr ago, its former position shows good agreement with the center of the shell (de Geus 1992), and this also support the scenario that the previous companion of  $\zeta$  Oph has exploded.

## 5. Summary

A summary of this paper is as follows:

1.  $^{12}\text{CO}$  ( $J = 1-0$ ) observations around the region of  $\zeta$  Oph of  $47 \text{ deg}^2$  have revealed two major filamentary cloud complexes (L156 and L204 complex) lying on the near-side of an H II region S27.
2. These cloud complexes are divided into 7 clouds whose masses range from  $70 M_\odot$  to  $520 M_\odot$  and their total mass is  $1630 M_\odot$ .
3. The denser parts of the cloud which are traced by  $^{13}\text{CO}$  and  $\text{C}^{18}\text{O}$  emission are located in the filaments facing  $\zeta$  Oph and the cloud complexes have peculiar velocity structures. These imply the physical interaction of the clouds and the H II region that the molecular gas is pushed and flown away from  $\zeta$  Oph.
4. We investigate the momentum and the kinetic energy for each molecular cloud. The cloud momentum and kinetic energy range  $60\text{-}800 M_\odot \text{ km s}^{-1}$  and  $(0.9\text{-}21) \times 10^{45}$  erg, respectively.
5. As the origin of the streaming motion, the stellar wind from  $\zeta$  Oph and UV photo dissociation effect are consid-

ered. The estimated time scales required for producing the momenta and kinetic energies of the clouds show that the stellar wind is hardly the cause of the gas acceleration while UV photo dissociation can be.

6. The cloud turbulent motion is suggested to be an important factor for the cloud evolution by previous studies. Our results indicate that the photo dissociation by a strong UV field may put the turbulent energy into the clouds and result in low star formation activity in this region if the contribution from other members of the Sco OB2 association is taken into account.

We would like to thank Ralph Neuhäuser, Yoshinori Yonekura and Nobuyuki Yamaguchi for very helpful comments on the manuscript. We greatly appreciate the hospitalities of all staff members of the Las Campanas Observatory of the Carnegie Institution of Washington. The NANTEN project is based on the mutual agreements between Nagoya University and Carnegie Institution of Washington. We also acknowledge that this project can be realized by the contribution from many Japanese public donors and companies. This work was financially supported in part by Grant-in-Aid for International Scientific Research from the Ministry of Education, Science, and Culture of Japan (No.10044076). Two of the authors (YF and AM) acknowledge financial support from the scientist exchange program under bilateral agreement between JSPS (Japan Society for the Promotion of Science) and CONICYT (the Chilean National Commission for Scientific and Technological Research).

**References**

- Bohlin, R.C. 1975, ApJ, 200, 402  
de Geus, E. J. 1992, A&A, 262, 258  
de Geus, E.J., de Zeeuw, P.T., Lub, J. 1989 A&A, 216, 44  
Dobashi, K., Bernard, J.P., Fukui, Y 1996, ApJ, 466, 282  
Draine, B.T. 1986 ApJ, 310, 408  
Gull, T.R., Sofia, S. 1979, ApJ, 230, 782  
Heiles, C. 1988, ApJ, 324, 321  
Hunter, S.D. et al. 1997, ApJ, 481, 205  
Kahn, F.D. 1969, Physica 41, 172  
Kawamura, A., Onishi, T., Yonekura, Y., Mizuno, A., Dobashi, K., Ogawa, H., Fukui, Y. 1998, ApJS, 117, 387  
Kopp, M., Gerin, M., Roueff, E., Le Bourlot, J. 1996, A&A, 305, 558  
Langer, W.D., Glassgold, A.E., Wilson, R.W. 1987, ApJ, 322, 450  
Lesh, J.R. 1968, ApJS, 17, 371  
Lynds, B.T. 1962, ApJS, 7, 1  
Liszt, H.S. 1997 A&A, 322, 962  
McCutcheon, W. H., Vrba, F. J., Dickman, R. L., Clemens, D. P. 1986, ApJ, 309, 619  
Morgan, W.W., Strömgren, B., Johnson, H.M. 1955, ApJ, 121, 611  
Morton, D.C. 1975, ApJ, 197, 85  
Nakano, T. 1998, ApJ, 494, 587  
Nozawa, S., Mizuno, A., Teshima, Y., Ogawa, H., Fukui, Y. 1991, ApJS, 77, 647  
Oort, J.H., Spitzer, L.Jr. 1955 ApJ, 121, 6  
Panagia, N. 1973 AJ, 78, 929  
Perryman, M.A.C. et al. 1997 A&A, 323, L49  
Preibish, T. , Zinnecker, H. 1999 AJ, 117, 2381  
Reipurth B. 1983, A&A, 117, 183  
Sivan, J.P. 1974, A&AS, 16, 163  
Tachihara, K., Dobashi, K., Mizuno, A., Ogawa, H., Fukui, Y. 1996 PASJ, 48, 489  
Tachihara, K., Mizuno, A., Fukui, Y. 2000 ApJ, 528, 817  
Van Buren, D., McCray, R. 1988, ApJ, 329, L93  
Weaver, R., McCray, R., Castor, J., Shapiro, P., Moore, R. 1977, ApJ, 218, 377  
Yonekura, Y., Dobashi, K., Mizuno, A., Ogawa, H., Fukui, Y. 1997, ApJS, 110, 21

Fig. 1. Integrated intensity map of  $^{12}\text{CO}$  ( $J=1-0$ ) emission line in the Galactic coordinate. Contours are drawn from  $1.2 \text{ K km s}^{-1}$  with  $2.4 \text{ K km s}^{-1}$  step. Dotted lines show the observed area in  $^{12}\text{CO}$ . Broken lines are the grids in the equatorial coordinate (B1950). Plus mark denote the position of  $\zeta$  Oph.

Fig. 2. Identification of the molecular clouds. Gray image is the integrated intensity of  $^{12}\text{CO}$  and the contours show the cloud boundaries. The solid lines divide the connected molecular clouds. Incompletely observed clouds are excluded. Dotted lines show the observed area in  $^{12}\text{CO}$ .

### Figure captions

Fig. 3. Close up images of L204 complex in  $^{12}\text{CO}$  (upper),  $^{13}\text{CO}$  (middle), and  $\text{C}^{18}\text{O}$  (lower). The lowest contour levels and contour intervals are  $1.2 \text{ K km s}^{-1}$  and  $2.4 \text{ K km s}^{-1}$  for  $^{12}\text{CO}$ ,  $1.6 \text{ K km s}^{-1}$  and  $1.6 \text{ K km s}^{-1}$  for  $^{13}\text{CO}$ , and  $0.18 \text{ K km s}^{-1}$  and  $0.18 \text{ K km s}^{-1}$  for  $\text{C}^{18}\text{O}$ , respectively. The observed areas in  $^{13}\text{CO}$  and  $\text{C}^{18}\text{O}$  are shown by the broken lines.  $^{13}\text{CO}$  clouds identified by Nozawa et al. (1991) and  $\text{C}^{18}\text{O}$  cores by Tachiahra et al. (1999) are denoted.

Fig. 4. Pseudo color images of channel maps in  $^{12}\text{CO}$ . Each map is integrated over  $\Delta V = 0.6 \text{ km s}^{-1}$ . The integrated velocity ranges are shown in each map. Star in each map shows the position of  $\zeta$  Oph.

Fig. 5. Pseudo color image of peak velocity of  $^{12}\text{CO}$  emission. Cross mark and arrow show the position and proper motion of  $\zeta$  Oph, respectively.

Fig. 7. Intensity distribution along the strip lines of A-B (a), C-D (b), and E-F (c). Intensity of  $^{12}\text{CO}$ ,  $^{13}\text{CO}$ ,  $\text{C}^{18}\text{O}$  and  $100\ \mu\text{m}$  are illustrated by solid, broken, dotted, and dash-dotted lines, respectively. The intensity scales are shown in the left side ( $^{12}\text{CO}$ ) and right side ( $^{13}\text{CO}$  and  $\text{C}^{18}\text{O}$ ), while  $100\ \mu\text{m}$  is arbitrary scaled.

Fig. 6. Intensity map of *IRAS*  $100\ \mu\text{m}$ . Contours of  $^{12}\text{CO}$  cloud boundaries are overlaid. Red circle show the extent of the H II region of S27. Three blue lines denote the strips where intensity distributions are investigated (see text and Figs. 7).